Investigation of γ'-Fe_4N−GaN Nanocomposites: Structural and Magnetic Characterization, Mössbauer Spectroscopy and Ab Initio Calculations

Sajith Kurian,[†] Sayan Bhattacharyya,*[,‡] Judith Desimoni,[§] Eitel L. Peltzer y Blancá,[⊥] Arles V. Gil Rebaza,[§] and N. S. Gajbhiye*[,†]

Department of Chemistry, Indian Institute of Technology, Kanpur 208016, U.P., India, Department of Chemical Sciences, Indian Institute of Science Education and Research, Kolkata, Mohanpur 741252, Nadia, W.B., India, Departamento de Física, Facultad de Ciencias Exactas, UNLP, IFLP-CONICET, CC 67, 1900 La Plata, Argentina, and Grupo de Estudio de Materiales y Dispositivos Electrónicos (GEMyDE), Facultad de Ingeniería, UNLP, IFLYSIB-CONICET, CC N° 565, 1900 La Plata, Argentina

Received: July 6, 2010; Revised Manuscript Received: August 28, 2010

A controlled, one-step ammonolysis method with three different Fe/Ga ratios (70:30, 50:50, and 30:70) was used to synthesize functional nanocomposite materials consisting of 30−40 nm particles of γ'-Fe_4N $Fe_{4-x}Ga_xN$ phases in a GaN and Fe-doped GaN phase matrix. The γ'-Fe_4N, $Fe_{4-x}Ga_xN$, and GaN phases were confirmed by the Rietveld analysis of the X-ray diffraction patterns, and the Fe-doped GaN phase was confirmed from Mössbauer spectroscopy and magnetization measurements. The magnetization of the superparamagnetic nanoparticles was expectedly reduced with the Ga incorporation in the samples. The coexistence of antiferromagnetic $Fe_{4-x}Ga_xN$ and the ferromagnetic γ'-Fe_4N phases resulted in an exchange bias effect (hysteresis loop shift of 28 Oe at 5 K) and a gradual magnetic phase transition from 250 to 55 K. Mössbauer spectroscopic analysis showed a hyperfine magnetic field distribution that the ab initio calculations duly supported. Ab initio calculations of the equilibrium lattice and Mössbauer hyperfine parameters were also performed.

Introduction

γ'-Fe_4N is a well-known soft ferromagnetic (FM) material, since it possesses high saturation magnetization with low coercivity, perfectly suitable for high-performance magnetic recording heads.[1] It adopts an antiperovskite type crystalline structure with space group *Pm*-3*m*, standard lattice parameter of $a = 3.7900$ Å.[2] To obtain additional functional properties and to improve the corrosion resistance and magnetic properties, especially coercivity, several studies have been carried out on the substitution of Fe atoms by different elements in the γ'-Fe_4N structure.[3] It has been found that the newly introduced metal atoms at Wyckoff positions 1*a* (corner of the cube, FeI) or 3*c* (center of the face, FeII)[4] control the crystal growth, thereby yielding magnetic particles with lower dimensions and pronounced anisotropic particles with high coercive fields, making the material suitable for high-density storage applications. The preferential substitution of the metal atoms at the 1*a* or 3*c* positions depends on the relative affinities of Fe or the metal atoms to nitrogen.[5]

The chemical affinity increases for atoms with atomic number lower than that of iron in the periodic table, and atoms with higher atomic number can be used to substitute iron in an ordered disposition. If the metallic radius of the substituting atom is larger than that of Fe, position 1*a* in the γ'-Fe_4N crystal lattice is clearly preferred because the coordination sphere of the 1*a*-centered cuboctahedron is larger than the one at the 3*c* position.[6] Gallium has a metallic radius of 1.41 Å[7] which is larger than that of iron (1.24 Å), so gallium will enter the 1*a* position in an ordered disposition to give $GaFe_3N$.[5] Although there are a number of literature reports available on the theoretical and experimental investigations of MFe_3N (M = Pd, Pt, Ir, Os, Rh, Sn, In, Zn, Ru, Co, Ni, Mn),[3] there is a scarcity of reports on $GaFe_3N$, except the first report on the synthesis of $GaFe_3N$ by Stadelmaier and Fraker in 1962[8] and the recent one by Houben et al.[6]

Houben et al. have shown that the replacement of the corner (1a) Fe atom in γ'-Fe_4N by Ga alters the magnetic nature of the system.[6] Upon incorporation of Ga into γ'-Fe_4N ($Fe_{4-x}Ga_xN$, $x \geq 0.5$), the ferromagnetic nature of pristine γ'-Fe_4N changes to antiferromagnetic (AFM) $GaFe_3N$. It has often been found that the formation of ternary iron nitrides is accompanied by the formation of an additional side phase, which is nearly unavoidable by normal synthesis procedures, similar to the secondary phase formation reported by Stadelmaier and Fraker for $GaFe_3N$[8] and by Kuhnen et al. in the synthesis of $ZnFe_3N$.[5] However, an improved synthesis method involving two-step ammonolysis has been proposed by Houben et al. for the synthesis of $RhFe_3N$,[3a] and $GaFe_3N$.[6] The secondary phase formation in these ternary nitride systems occurs due to slow reaction of iron to form the alloy and also the lower free energy of formation of binary nitrides as compared with the ternary ones. The one-step ammonolysis of oxide nanoparticles in a conventional nitridation furnace and the control of the synthesis parameters allow the effective tuning of the magnetic properties of the nanocomposites. A perfect control and the knowledge of the magnetic interactions present in these functional nanocomposites is essential to tune the properties for applications in magnetic recording media and data storage devices.[9] It is noteworthy to mention here that in our previous work, introduction of Ga in ε-Fe_3N resulted in pseudo-binary ε-$Fe_{3-x}Ga_xN$ phases at low Ga

* Corresponding author. E-mail: sayanb@iiserkol.ac.in (S.B.); nsg@iitk.ac.in (N.S.G.).
[†] Indian Institute of Technology.
[‡] Indian Institute of Science Education and Research.
[§] IFLP-CONICET, CC 67.
[⊥] IFLYSIB-CONICET, CC N° 565.

10.1021/jp106221w
Published on Web 09/24/2010

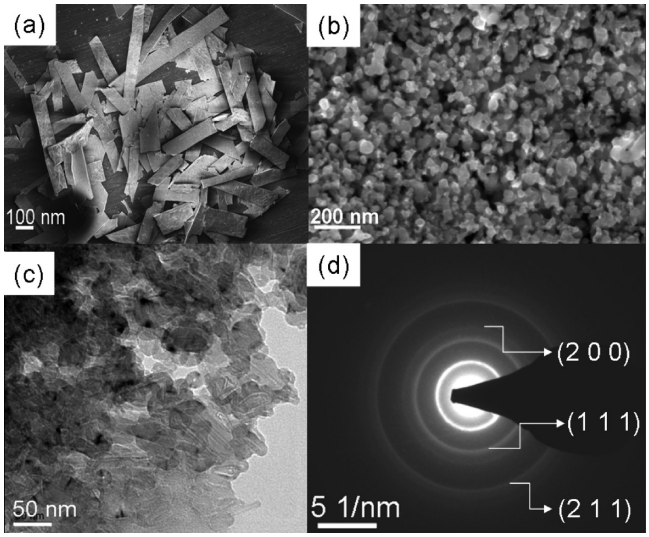

Figure 1. FESEM image of the nanocomposite with 70:30: Fe/Ga composition showing (a) strip like morphology at low magnification, (b) individual spherical nanoparticles within the strips, (c) TEM image of the particles and (d) the SAED pattern.

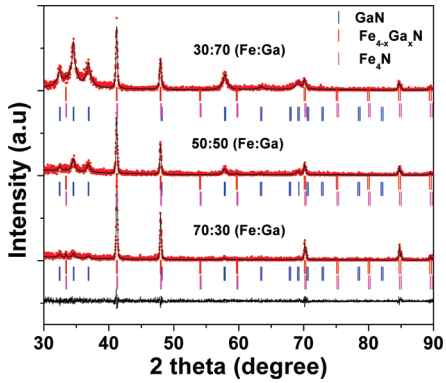

Figure 2. Refined XRD pattern of the nanocomposite samples.

concentrations ($x \sim 0.2$), whereas core−shell ε-Fe_3N-GaN nanocomposites were obtained at higher Ga concentrations.[10]

In this study, we report on three compositions of γ'-Fe_4N/$Fe_{4-x}Ga_xN$ nanoparticles embedded in a GaN matrix, according to the initial Fe/Ga atomic ratios of 70:30, 50:50, and 30:70. The synthesis was carried out by a controlled one-step ammonolysis of oxide nanoparticles in a conventional nitridation furnace. The synthesis parameters were tuned to have a ferromagnetic (FM) core of γ'-Fe_4N and an antiferromagnetic (AFM) shell/matrix of $Fe_{4-x}Ga_xN$, which ultimately results in an exchange-coupled system of γ'-Fe_4N/$Fe_{4-x}Ga_xN$ phases embedded in the GaN matrix. Structural, magnetic, and hyperfine characterizations are put together with the ab initio calculations[1a,11] of equilibrium lattice constants, magnetic moments, and hyperfine parameters to ascertain the compositional and functional properties of the present nanocomposite system.

Results

Structural Characterization. Figure 1 shows a typical Field emission scanning electron microscopic (FESEM) image of the

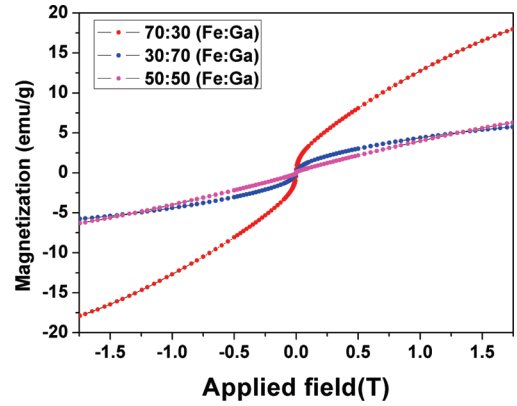

Figure 3. Magnetization as a function of field at 300 K.

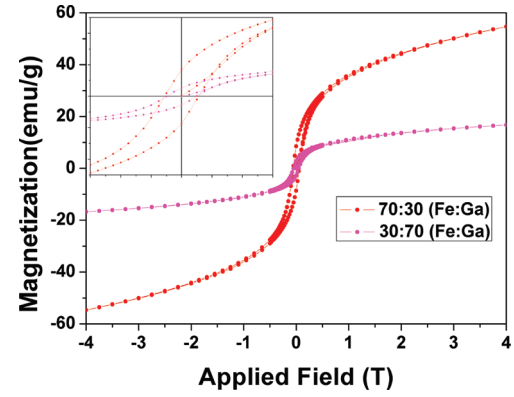

Figure 4. Magnetization as a function of field at 5 K.

70:30 (Fe/Ga) nanocomposite γ'-Fe_4N/$Fe_{4-x}Ga_xN$ sample. A strip-like morphology at lower magnification is observed in Figure 1a. The strips are composed of small spherical ~30 nm sized particles (Figure 1b). The TEM image in Figure 1c displays the 30−40 nm spherical particles accompanied by a smaller fraction of tube-like nanostructures. The different contrast detected within these tube-like structures resembles a core−shell-like morphology resembling the different phases. The selected area electron diffraction (SAED) pattern in Figure 1d is indexed to the γ'-Fe_4N phase, although a clear distinction could not be obtained between the lattice spacing of γ'-Fe_4N and $Fe_{4-x}Ga_xN$ phases.

To get a clear picture of the different phases present and their weight percentages, Rietveld refinement was performed on the X-ray diffractograms (XRDs) displayed in Figure 2. According to the analysis, all the samples are composed of a well ordered phase analogous to γ'-Fe_4N structure. A careful observation towards lower diffraction angles reveals the presence of three peaks at $2\theta = 32.4$, 34.5, and 36.8° corresponding to the hexagonal GaN phase that is almost buried in the background of the diffractogram of the 70:30 sample. The Rietveld refinement of the XRD patterns enabled the identification of the three separate phases: γ'-Fe_4N, $Fe_{4-x}Ga_xN$, and GaN, appropriately corroborated with the observed magnetic and Mössbauer results, discussed later. The refinement of the diffractograms also allows us to discard the possibility of other alloy phases, such as Fe_3Ga,

TABLE 1: Refined XRD Parameters

	occupancy of 1*a* position		lattice parameter (Å)			wt %		
(Fe/Ga)	Fe	Ga	$Fe_{4-x}Ga_xN$	Fe_4N	GaN	$Fe_{4-x}Ga_xN$	Fe_4N	GaN
70:30	0.384	0.616 (2)	3.7930 (1)	3.79	3.1901 (1) 5.1906 (8)	51 (4)	47 (2)	2 (0)
50:50	0.325	0.675 (4)	3.7951 (1)	3.79	3.1897 (1) 5.1941 (3)	12 (2)	4 (1)	84 (14)
30:70	0.320	0.680 (7)	3.7957 (2)	3.79	3.1866 (6) 5.1928 (4)	2 (0)	1 (0)	97 (8)

TABLE 2: Magnetic and Mössbauer Data of the Samples at 293 and 5 K[a]

	magnetization data				Mössbauer data[b]		
	293 K		5 K		293 K	5 K	
(Fe/Ga)	magnetization at 1.75 T (emu/g)	Hc (Oe)	magnetization at 4 T (emu/g)	Hc (Oe)	δ (mm/s)	δ (mm/s)	2ε (mm/s)
70:30	17	28	55	562	0.22	0.44	0.26
50:50	6	5	24	702	0.25	0.49	0.10
30:70	5	13	17	490	0.23	0.43	0.18

[a] At 293 K is reported the fitted isomer shift value (δ) of the quadrupolar distribution; at 5 K are quoted the isomer (δ) and quadrupole (2ε) shifts of the hyperfine field distribution. [b] Error in the values is within ±0.05 mm/s.

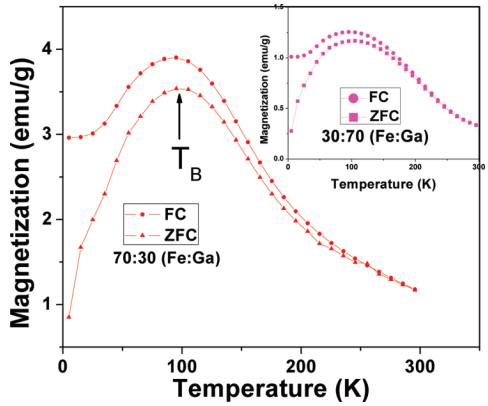

Figure 5. ZFC/FC curves at an applied field of 0.01 T for 70:30 Fe/Ga samples.

$FeGa_3$ and Fe_6Ga_2. In the analysis process, the lattice parameter of the γ'-Fe_4N phase has been constrained as 3.7900 Å,[2] and that of other phases were allowed to vary. In addition, the occupation number of the 1*a* site was permitted to refine by constraining the total occupancy as 1. The lattice parameters and the occupation numbers for each phase are given in Table 1.

Magnetic Characterization. Room temperature DC magnetization measurements were performed for all the samples with different compositions. From the nature of the obtained hysteresis curves (Figure 3), it is observed that the 30:70 and 50:50 Fe/Ga samples are close to being paramagnetic, whereas the 70:30 sample shows a superparamagnetic behavior. The room temperature (RT) hysteresis loops of all the three samples remain unsaturated up to 1.75 T applied field, although the center of the loops show an "s" type shape, characteristic of a FM material. The 70:30 sample has a magnetization value of 17 emu/g at RT; the other two samples have an almost equal magnetization value of 6 emu/g at a field of 1.75 T. As expected, the magnetization data at 5 K (Figure 4) shows a remarkable enhancement in the coercivity values as given in Table 2. The ZFC and FC curves (Figure 5) measured at 0.01 T clearly show a broad maximum at ~90 K, which can likely be ascribed to the superparamagnetic blocking temperature.

Hyperfine Characterization. For all samples, Mössbauer spectra recorded at RT show an asymmetric doublet, in accord with the observed magnetic behavior discussed in the previous section. A typical spectrum of the 70:30 (Fe/Ga) sample is shown in Figure 6. Considering the various phases present in the sample, we fitted the set of spectra with a quadrupolar distribution, as plotted in the right of Figure 6. In all cases, the maximum of the probability distribution is centered at 0.6 mm/s, and the average isomer shift is 0.24 mm/s. The spectra obtained at 5 K (Figure 7) are characterized by complex structures, suggesting the superposition of distributed magnetic interactions. Since it was impossible to deconvolute the spectra taking into account the characteristic three sextets of γ'-Fe_4N[1a] and the other possible sextets/doublets corresponding to the $Fe_{4-x}Ga_xN$ and Ga(Fe)N components, the spectra were reproduced using a hyperfine field distribution, including a nonvanishing probability at zero field to take into account the nanoparticle size effect on the magnetic behavior of the phases. The result of the fitting procedure is presented in Figure 7, along with the corresponding hyperfine field probability distributions. The fitted average isomer and quadrupole shift values are reported in Table 2.

Ab Initio Calculations. To find the magnetic and structural equilibrium configuration of the $Fe_{4-x}Ga_xN$ system, different Fe−Ga−N configurations that gave rise to the superlattices displayed in Figure 8 were considered, and the total energy curves vs lattice parameter were determined for the different superlattices. The resulting total energy vs lattice parameter curves of the different Ga concentrations are displayed in Figure 9. The curves show the usual smooth behavior and were fitted with the Murnaghan's equation[12] (solid lines in the figure). In the case of $x = 0.750$ (inset in Figure 9a), the lowest energy magnetic configuration corresponds to the configuration labeled as 8-a in Figure 8.

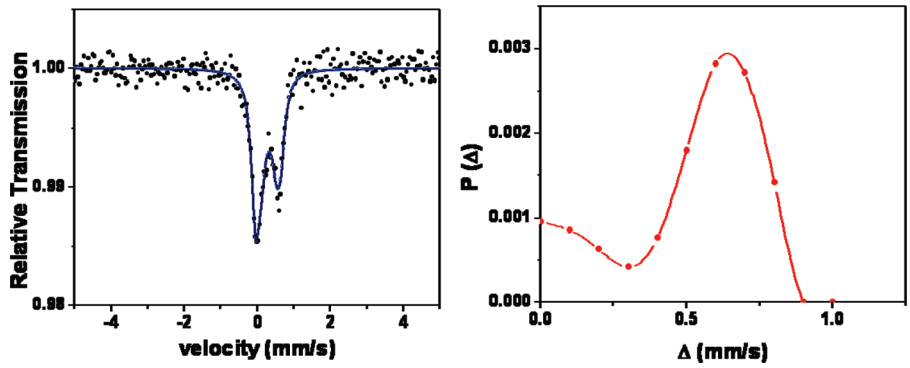

Figure 6. Mössbauer spectrum (left) of the 70:30 (Fe/Ga) sample at 300 K and (right) the quadrupolar probability distribution.

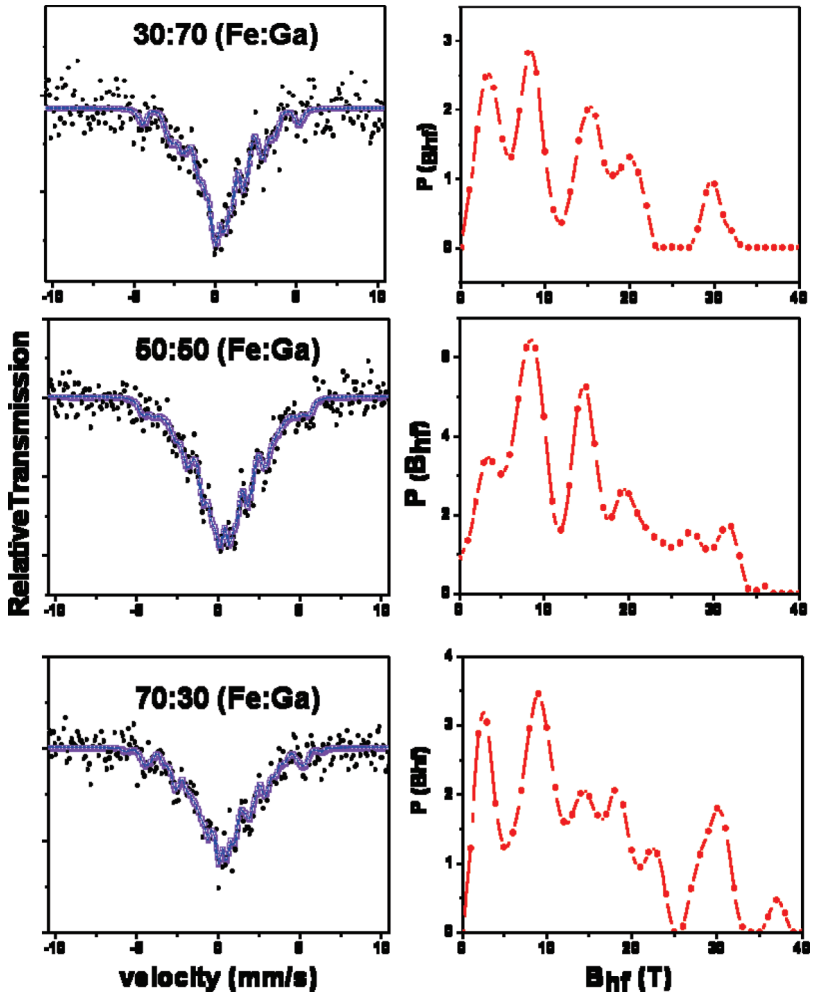

Figure 7. Mössbauer spectra (left) of samples at 5 K with the hyperfine field distribution probability (right).

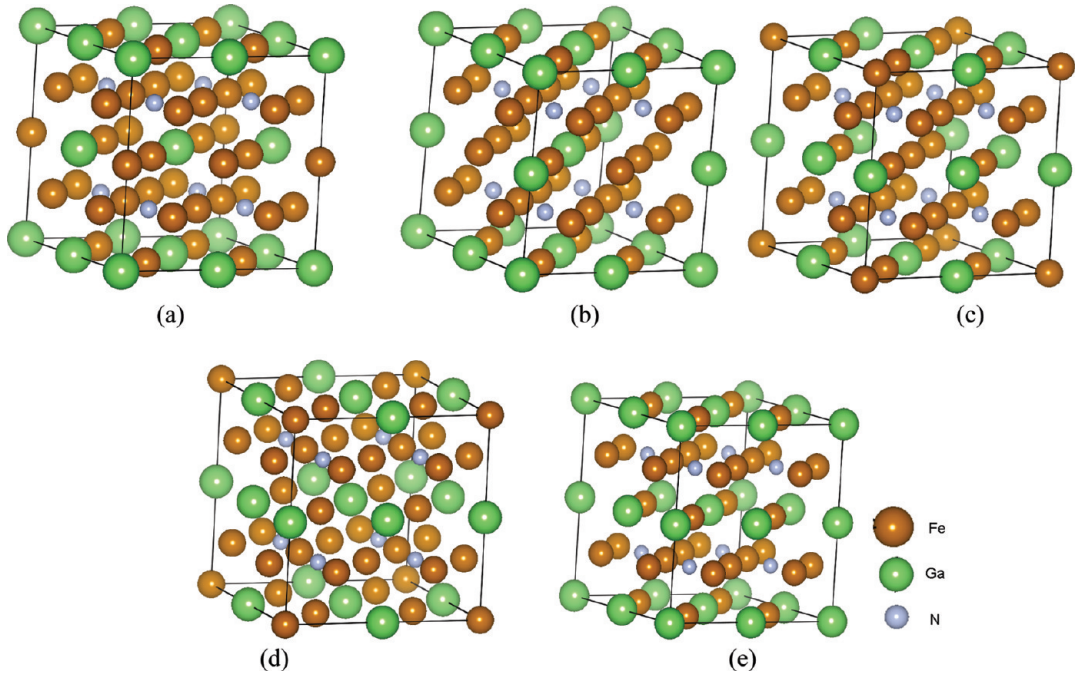

Figure 8. Superlattices used for the calculations: (a−c) $x = 0.750$, (d) $x = 0.875$, and (e) $x = 1.000$.

It is observed from Figure 9 that the magnetically ordered structure is the ground state $Fe_{4-x}Ga_xN$ phase for all concentrations; the atomic magnetic moment of Ga and Fe are antiparallel, lying in the [001] direction, giving an AFM ordered structure. The calculated equilibrium structural, magnetic, and hyperfine parameters are given in Table 3. The previous results obtained

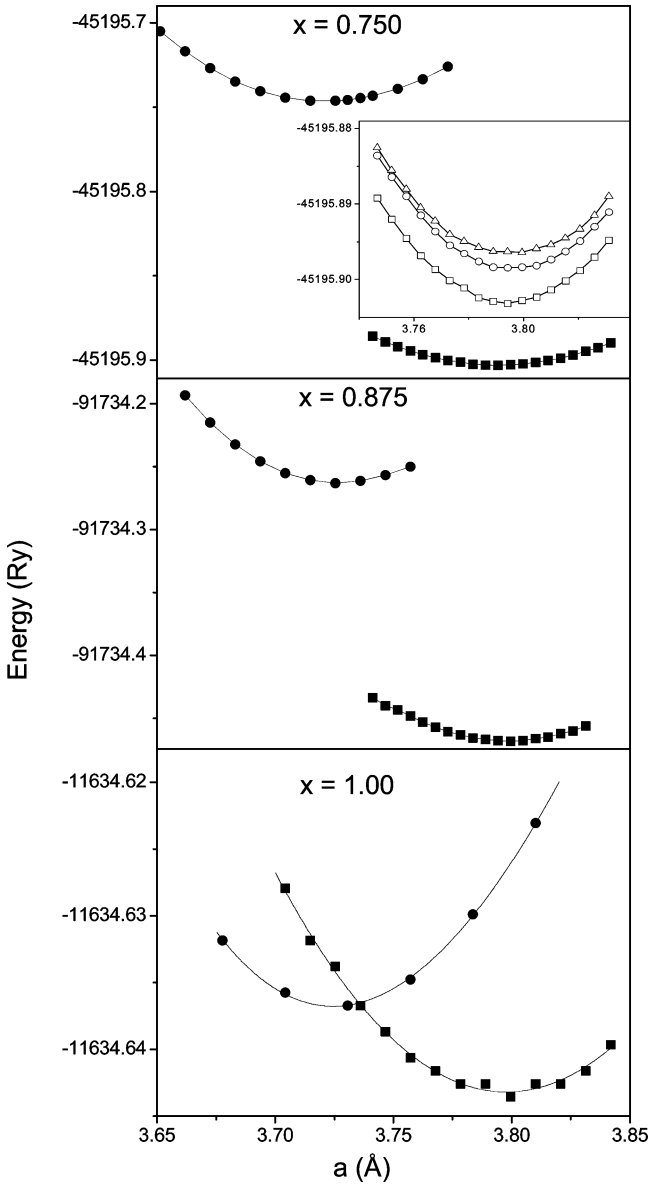

Figure 9. Energy vs lattice parameter labeled with the Ga concentration. (a) Squares: magnetic phase calculations. (b) Circles: nonmagnetic phase calculations. The inset corresponds to the three configurations corresponding to $x = 0.75$ (open squares, open circles, and open triangles correspond to a, b, c supercells of Figure 8).

for the Fe_4N phase ($x = 0.000$) are also included in Table 3.[1a] In all cases, the magnetic hyperfine field points in the [00$\bar{1}$] direction, whereas the main component of the electric field gradient lies in the [001] direction.

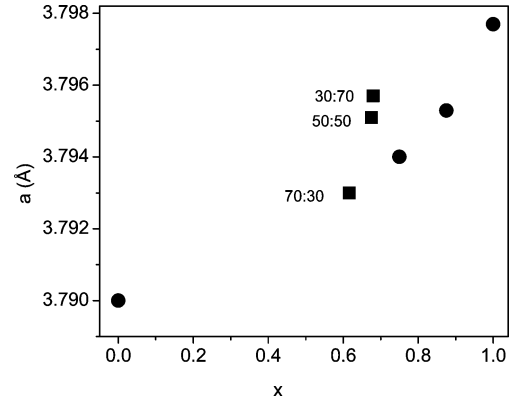

Figure 10. Lattice parameter vs Ga concentration: (a) squares, present XRD determinations; (b) circles, equilibrium lattice constants obtained from the ab initio calculations.

Discussion

Due to the low solubility of Ga in Fe and the low free energy of formation of hexagonal GaN phase, the synthesis of the nanocomposites was accompanied by the formation of GaN. To obtain single phase ternary nitride, a two-step ammonolysis method is required with a high-temperature sintering step and a low-temperature nitridation reaction.[6] However, since our aim is to study the magnetic behavior of the nanocomposites comprising FM, AFM, and diamagnetic phases, we avoided sintering the samples. In this system, the two phases, γ'-Fe_4N and GaN, were formed separately, followed by the diffusion of Ga atoms into the γ'-Fe_4N lattice, partially replacing the Fe atoms at the 1*a* positions. This results in the formation of $Fe_{4-x}Ga_xN$ phase surrounding γ'-Fe_4N. As is evident from the evolution with Ga content of the refined occupation numbers and the lattice parameters of $Fe_{4-x}Ga_xN$ phase, the occupancy of Ga increases at the 1*a* site with a change in the Fe/Ga ratio from 70:30 to 30:70. There is a slight variation in the observed occupation number and the lattice parameters from the 50:50 to 30:70 compositions of Fe/Ga. In a simple picture and owing to the larger atomic radii of Ga atoms compared with Fe (1.41 and 1.26 Å, for Ga and Fe, respectively), an increment of the lattice parameter should be expected due to the replacement of Fe by Ga atoms at the lattice sites. Moreover, the agreement of the lattice parameters obtained from ab initio calculations and the experimental ones, as observed in Figure 10, reinforce the hypothesis of the formation of $Fe_{4-x}Ga_xN$. On the other hand, the presence of various phases in the samples clearly indicates that the reaction temperature is not sufficient for the effective diffusion of Ga atoms within the γ'-Fe_4N lattice and to fully replace the 1*a* Fe atoms.

The lack of saturation of hysteresis loops of all samples (Figure 3), even at a field of 1.75 T, is due to the AFM character

TABLE 3: Ab Initio Calculated Lattice Parameters (*a*), and Bulk Modulus (*B*), Magnetic Moments (μ), Relative Fraction of Sites (*f*), Hyperfine Field (B_{hf}), Quadrupolar Shift (2ε), and Isomer Shift (δ)[a]

composition	$x = 0.000$		$x = 0.750$				$x = 0.875$				$x = 1.000$			
a (Å)	3.7900		3.7940				3.7953				3.7977			
B (GPa)	200		167				177				217			
μ_{Ga} (μ_B)			−0.12				−0.12				−0.12			
	FeI	FeII	FeI	FeIIa	FeIIb	FeIIc	FeI	FeIIa	FeIIb	FeIIc	FeI	FeIIa	FeIIb	FeIIc
f (%)	25	50/25	7	31	31	31	4	48	48				100	
μ_{Fe} (μ_B)	2.84	2.27	2.83	1.82	1.71	1.92	2.87	1.85	1.74				1.76	
B_{hf} (T)	36.9	23.8	37.6	19.8	17.7	21.3	39.3	19.9	17.9				17.9	
δ (mm/s)	0.48	0.42	0.29	0.44	0.47	0.41	0.28	0.44	0.47				0.48	
2ε (mm/s)	0.00	0.27/0.54	−0.09	0.84	1.05	0.69	0.00	0.86	1.04				103	

[a] The $x = 0.00$ values are taken from ref 1a.

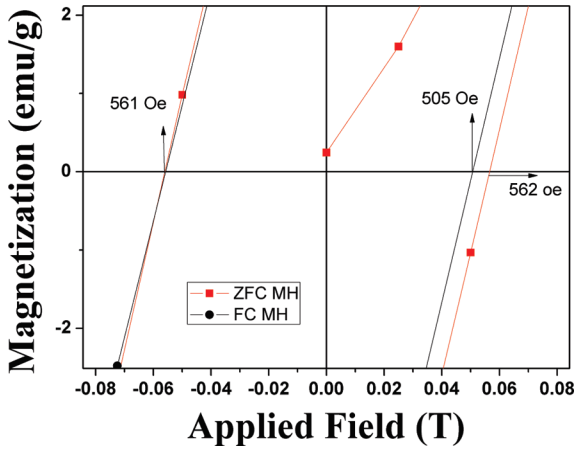

Figure 11. Magnetization as a function of field measured after cooling in zero field and an applied field of 2 T.

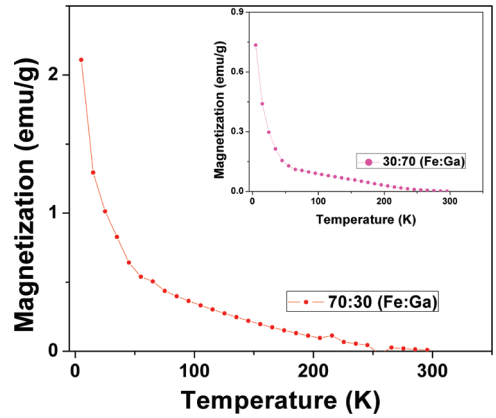

Figure 12. FC−ZFC curve of the 70:30, and 30:70 Fe/Ga samples.

of the $Fe_{4-x}Ga_xN$ phase coupled with the FM behavior of the γ'-Fe_4N phase. The presence of the additional GaN phase also contributes to lowering of the saturation magnetization. At 5 K and an applied field of 4 T, the hysteresis curves are still not saturated. The center ferromagnetic part is dominated by the γ'-Fe_4N phase, and the unsaturated behavior originates from the AFM $Fe_{4-x}Ga_xN$ phase, accompanied by superparamagnetic fractions of the ∼30 nm particles.

The combination of the soft FM γ'-Fe_4N phase with the AFM $Fe_{4-x}Ga_xN$ phase can exhibit exchange bias coupling of the respective spins at the AFM/FM interface at low temperature, resulting in an enhanced coercivity.[13] Bulk γ'-Fe_4N has a coercivity of 5 Oe;[14] the reported values of coercivity of γ'-Fe_4N nanoparticles of size 60−80 nm is 40−60 Oe;[15] and the AFM $Fe_{4-x}Ga_xN$ phase has a negligible coercivity, as reported by Houben et. al.[6] However, the behavior of the hysteresis loops recorded at 5 K (Figure 4) clearly suggests the single domain nature of core γ'-Fe_4N and the existence of an exchange bias effect at the interface of the FM γ'-Fe_4N and AFM $Fe_{4-x}Ga_xN$ phases. In fact, the hysteresis loop is shifted by 0.0028 T toward the negative field direction after cooling the sample with an applied field of 2 T (Figure 11). As a cross-check, cooling the sample under zero field did not result any loop shift.

The broad nature of the peaks in the ZFC and FC curves (Figure 5) can be associated with the large particle size distribution in the nanocomposites. The maximum at 90 K is due to the superparamagnetic blocking temperature of the FM phase(s). The nature of the ZFC/FC curves clearly shows a dominant FM contribution as compared with the weaker AFM interactions. There is no clear indication of Néel temperature, even for the bulk pure AFM $GaFe_3N$,[6] and in addition, the inverse susceptibitility curve exhibits only a slightly negative Curie−Weiss temperature dependence. But unlike the normal ZFC and FC curves for FM nanoparticles, the observed ZFC/FC curves start bifurcating at a higher temperature, ∼250 K.

For an isolated FM material, the difference curves of FC and ZFC quickly drop to zero magnetization above the blocking temperature, whereas the observed magnetization vs temperature curve of the 70:30 and 30:70 samples (Figure 12) has a slow magnetization decay between 55 and 250 K after a quick drop up to 50 K.[16] This implies a secondary magnetic phase transition in the systems. The observed trend can be due to the AFM-to-partial-FM transition of the $Fe_{4-x}Ga_xN$ phase. In the crystalline AFM $Fe_{4-x}Ga_xN$ lattice, coupling of the nearest-neighbor spins can lead to ferro-/ferrimagnetic ordering at lower temperatures, depending on the equivalent/nonequivalent cation sublattices. This magnetic transition is speculatively gradual, with an onset from 250 ± 20 K, the deviation point of the ZFC and FC curves, until around 55 K. An additional contribution to the observed behavior is from the blocking of superparamagnetic spins of a Fe-doped GaN phase, supported by low-temperature Mössbauer results that will be presented and discussed later. It is well-known that doping of transition metals such as Fe, Mn, etc. can convert an otherwise diamagnetic GaN (bulk[17]) to a weakly FM material in the nanosize regime.[18]

The room temperature superparamagnetic behavior of the samples as observed from the magnetization experiments are duly corroborated by the asymmetric doublet observed in the room temperature Mössbauer spectrum presented in Figure 6. The Mössbauer spectra recorded at 5 K (Figure 7) show a complex structure that was reproduced with a distribution of the hyperfine field with several maxima at ∼3, 9, 15, 19, 28, and 36 T for all samples. In the case of the 70:30 sample, a maximum at around 23 T is also detected in the field distribution. Such a complex Mössbauer spectra originates from the Ga concentration gradient with the consequent setting up of different Fe−Ga−N configurations with similar hyperfine interactions.

To support the interpretation of such a complex distribution, we have used ab initio calculations, focusing the comparisons only in the hyperfine field, since the fitted values of the isomer and quadrupole shifts are a global average. From Table 3, it is observed that the FeI interaction is very close to the one associated with the FeI site of the γ'-Fe_4N phase.[1a] In addition, FeIIc interaction is observed only in the calculation performed for $x = 0.750$, the parameters of which are quite similar to the FeII interaction of the γ'-Fe_4N phase.[1a] The other interactions resulted exclusively from the $Fe_{4-x}Ga_xN$ phase.

By comparing hyperfine field distribution maxima with the calculated ones, a nice agreement is observed, so it is possible to directly associate the maxima of the distribution with the calculated hyperfine field. FeI and FeIIc hyperfine fields (36 and 23 T) are shared between the γ'-Fe_4N and $Fe_{4-x}Ga_xN$ phases; the other maxima (15, 19 T) can be ascribed to the FeIIb and FeIIa sites in the mixed Ga-substituted iron nitride. The maxima observed at around 3 and 8.5 T may be associated with the existence of (i) Fe doped into the GaN matrix;[19] (ii) the remaining superparamagnetic phases magnetically disordered, even at 5 K; or (iii) nonstoichiometric pure[20] or (iv) other substituted iron nitrides. It is worth mentioning that hyperfine distributions can be qualitatively reproduced considering the weight percentages obtained from the XRD results (Table 1), together with the relative fractions of the different iron sites in the superlattices used for the calculations (Table 3).

Conclusions

Fine tuning of an otherwise normal synthesis method involving the nitridation of gallium iron oxide particles produces the nanocomposite system consisting of γ'-Fe_4N, $Fe_{4-x}Ga_xN$, GaN, and Fe-doped GaN (in minute proportions). The relative weight percentages of the former two phases decreases with increasing Ga concentration. Global analysis of the results indicates nanoparticles consisting of a FM core of the γ'-Fe_4N phase covered by AFM $Fe_{4-x}Ga_xN$, the total ensemble within the GaN matrix, and a small percentage of Fe-doped GaN. The interaction between the spins at the AFM−FM interface results in an exchange bias effect. Analysis of the magnetism data points out the superparamagnetic blocking of γ'-Fe_4N spins, strong interaction between the FM γ'-Fe_4N and AFM $Fe_{4-x}Ga_xN$ phases, and AFM-to-partial-FM transition of the $Fe_{4-x}Ga_xN$ phase. Even though the Mössbauer spectra at 5 K shows a complex structure, existence of all the phases is confirmed by analysis of the spectra and the magnetic hyperfine fields obtained from the ab initio calculations.

Experimental Details

Materials. $Fe(NO_3)_3 \cdot 9H_2O$ (99.9%, SD Fine Chemicals), metallic Ga, citric acid (99.9%, Merck).

Methodology. The composite nanoparticles were synthesized by a combined reduction−nitridation method.[21] Stoichiometric amounts of $Fe(NO_3)_3 \cdot 9H_2O$ and $Ga(NO_3)_3 \cdot 9H_2O$ were dissolved in deionized water and mixed and stirred for 12 h to obtain a homogeneous solution. Three percentage compositions of 70:30, 50:50, and 30:70 of Fe/Ga were achieved by maintaining a slight excess of Ga atoms, which will ensure the simultaneous formation of GaN and $Fe_{4-x}Ga_xN$ phases. A saturated solution of citric acid was added to the mixed metal−salt solution dropwise with stirring. The resulting solution was stirred for 24 h to allow effective complexation. The metal-to-citric acid ratio was maintained at 1:1. After 24 h, the solution was slowly evaporated in a water bath at 363 K. The micrometer-sized fibers formed at the inner surface of the container were collected and heated in a furnace at 873 K for 4 h to convert the metal citrate complex to mixed metal oxides of Fe and Ga. The oxide nanoparticles were subsequently treated with high-purity NH_3 in a cylindrical furnace at 973 K for 8 h with a flow rate of 14 cm^3/min. After completion of the reaction, the product was quenched in water by maintaining the same flow rate as before.

Characterization. The as-synthesized particles were characterized by X-ray diffraction (Thermoelectron Corporation, ARL X-Tra) using Cu Kα radiation. The data were analyzed by the Rietveld method using the program FullProf-suite and a Pseudo-Voigt profile function.[22] Morphology and the size of the particles were determined by field emission scanning electron microscopy (FEI Quanta 200) and transmission electron microscopy (FEI Technai 20). Room temperature magnetic measurements were carried out using a vibrating sample magnetometer (DMS ADE-EV7 model). Low-temperature magnetic measurements were carried out by a superconducting quantum interference device (Quantum Design, model MPMS-XL). Room temperature Mössbauer measurements were performed using a ^{57}Co source incorporated in a Rh matrix with a commercial spectrometer supplied by Wissel. The measurements at 5 K were performed in a He bath cryostat. The spectra were analyzed by WinNormos software.[23]

Ab Initio Calculations Details. The γ'-Fe_4N has an antiperovskite structure (space group *Pm*-3m (221)) in which the Fe atoms occupy two distinguishable sites, the corners (FeI) and the center of the faces (FeII), and the N atoms are placed at the center of the cube.[4] To execute the calculations, $2 \times 2 \times 2$ superlattices were used, building up different superlattices from a Fe_4N superlattice with 8 FeI and 24 FeII atoms. To achieve the $x = 0.750$, 0.875, and 1.000 Ga concentrations, the FeI atoms were substituted by Ga atoms in Ga/Fe ratios of 2:6, 7:1, and 8:0, respectively. These substitutions give rise to different superlattices, three for $x = 0.750$ and only one for $x = 0.875$ and 1.000, giving rise to different neighborhoods for the Fe atoms which have been labeled as FeI (1*a* site) and FeIIa, FeIIb, and FeIIc (3*c* site).[4] The calculations were performed using the FP-LAPW method within the framework of density functional theory[24] as implemented in the Wien2K code.[25] In this framework, the exchange-correlation potential for structural and electronic properties were calculated using both a local spin density approximation and the generalized gradient approximation based on the Perdew−Burke−Ernserhof expression.[24d,26] The parameter $R_{MT}K_{max}$ was kept equal to 9 (R_{MT} is the muffin-tin radius, and K_{max} is the largest K vector in the plane wave expansion). The muffin-tin radii used for Ga, Fe, and N were 2.59, 1.79, and 1.59 bohr, respectively. A mesh of 286 k-points was taken in the irreducible wedge of the Brillouin zone. The total energy was converged to 10^{-6} Ry. In all calculations, relativistic effects and spin polarization were considered. Nonmagnetic and magnetically ordered configurations were considered.

Acknowledgment. S.K. and N.S.G. acknowledge financial assistance from DST, New Delhi, India. S.B. acknowledges infrastructure and facilities provided by IISER-K. The authors thank the UGC-DAE Consortium for Scientific Research, Indore for performing the Mössbauer spectra at 5 K with 5 T field. Research Grant PIP 5283 from Consejo Nacional de Investigaciones Científicas y Técnicas (CONICET, Argentina) and PICT 38047 and PICT 2042 from the Agencia Nacional de Promoción Científica y Tecnológica are gratefully recognized.

References and Notes

(1) (a) Peltzer y Blancá, E. L.; Desimoni, J.; Christensen, N. E.; Emmerich, H.; Cottenier, S. *Phys. Status Solidi, B* **2009**, *246*, 909–928. (b) Costa-Kramer, J. L.; Borsa, D. M.; Garcia-Martin, J. M.; Martin-Gonzalez, M. S.; Boerma, D. O.; Briones, F. *Phys. Rev. B* **2004**, *69*, 144402/1–144402/8. (c) Gallego, J. M.; Grachev, S.Yu.; Borsa, D. M.; Boerma, D. O.; Ecija, D.; Miranda, R. *Phys. Rev. B* **2004**, *70*, 115417/1–115417/11. (d) Appolaire, B.; Goune, M. *Comput. Mater. Sci.* **2006**, *38*, 126–135. (e) Teixeira, C. B.; Olavo, L. S. F.; Neto, K. S.; Morais, P. C. *Hyperfine Interact.* **2008**, *175* (1−3), 113–120. (f) Narahara, A.; Ito, K.; Suemasu, T.; Takahashi, Y. K.; Ranajikanth, A.; Hono, K. *Appl. Phys. Lett.* **2009**, *94* (20), 202502/1–202502/3. (g) Pelka, R.; Moszynska, I.; Arabczyk, W. *Catal. Lett.* **2009**, *128* (1−2), 72–76.

(2) Jacobs, H.; Rechenbach, D.; Zachwieja, U. *J. Alloys Compd.* **1995**, *227*, 10–17.

(3) (a) Houben, A.; Muller, P.; von Appen, J.; Lucken, H.; Niewa, R.; Dronskowski, R. *Angew. Chem., Int. Ed.* **2005**, *44*, 7212–7215. (b) Andriamandroso, D.; Matar, S.; Demazeau, G.; Fournes, L. *IEEE Trans. Magn.* **1993**, *29*, 2–6. (c) Matar, S.; Fournes, L.; CheRubin-Jeannette, S.; Demazeau, G. *Eur. J. Solid State Inorg. Chem.* **1993**, *30*, 871–881. (d) Siberchicot, B.; Matar, S. F.; Fournes, L.; Demazeau, G.; Hagenmuller, P. *J. Solid State Chem.* **1990**, *84*, 10–15. (e) Zhao, Z. J.; Xue, D. S.; Li, F. S. *J. Magn. Magn. Mater.* **2001**, *232*, 155–160.

(4) Jack, K. H. *Proc. R. Soc. London, Ser. A* **1951**, *208*, 216–224.

(5) Kuhnen, C. A.; de Figueiredo, R. S.; dos Santos, A. V. *J. Magn. Magn. Mater.* **2000**, *219*, 58–68.

(6) Houben, A.; Burghaus, J.; Dronskowski, R. *Chem. Mater.* **2009**, *21*, 4332–4338.

(7) Pauling, L. *J. Am. Chem. Soc.* **1947**, *69*, 542–553.

(8) Stadelmaier, H. H.; Fraker, A. C. *Z. Metallkd.* **1962**, *53*, 48–51.

(9) (a) Kume, M.; Tsujioka, T.; Matsuura, K.; Abe, Y.; Tasaki, A. *IEEE Trans. Magn.* **1987**, *MAG-23*, 3633–3635. (b) McFadyen, I. R.; Fullerton, E. E.; Carey, M. J. *Mater. Res. Bull.* **2006**, *31*, 379–383. (c) Moser, A.; Takano, K.; Margulies, D. T.; Albrecht, M.; Sonobe, Y.; Ikeda, Y.; Sun, S.; Fullerton, E. E. *J. Phys. D: Appl. Phys.* **2002**, *35*, R157–R167.

(10) (a) Gajbhiye, N. S.; Bhattacharyya, S. *J. Appl. Phys.* **2007**, *101*, 113902/1−113902/4. (b) Gajbhiye, N. S.; Bhattacharyya, S. *Nanotechnology* **2005**, *16*, 2012–2019.

(11) (a) Herper, H. C.; Hoffmann, E.; Entel, P. *Phys. Rev. B* **1999**, *60*, 3839–3848. (b) Kuhnen, C. A.; de Figueiredo, R. S.; Drago, V. *J. Magn. Magn. Mater.* **1992**, *111*, 95–104.

(12) Murnaghan, F. D. *Finite Deformation of an Elastic Solid*: John Wiley and Sons, Inc.: New York, 1951.

(13) (a) Ong, Q. K.; Wei, A.; Lin, X. M. *Phys. Rev. B* **2009**, *80*, 134418/1–134418/6. (b) Makhlouf, S. A.; Parker, F. T.; Spada, F. E.; Berkowitz, A. E. *J. Appl. Phys.* **1997**, *81* (8), 5561–5563. (c) Zeleňáková, A.; Kováč, J.; Zeleňňk, V. *Acta Phys. Pol., A* **2009**, *115* (1), 357–359.

(14) Chen, S. K.; Jin, S.; Tiefel, T. H.; Hsieh, Y. F.; Gyorgy, E. M.; Johnson, D. W., Jr. *J. Appl. Phys.* **1991**, *70* (10), 6247–6249.

(15) (a) Wu, X. L.; Zhong, W.; Jiang, H. Y.; Tang, N. J.; Zou, W. Q.; Du, Y. W. *J. Magn. Magn. Mater.* **2004**, *281*, 77–81. (b) Kurian, S.; Gajbhiye, N. S. *Hyperfine Interact.* **2008**, *183*, 147–153.

(16) (a) Jeon, Y.; Lee, G. H.; Park, J.; Kim, B.; Chang, Y. *J. Phys. Chem. B* **2005**, *109*, 12257–12260. (b) Pearton, S. J.; Overberg, M. E.; Thaler, G.; Abernathy, C. R.; Theodoropoulou, N.; Hebard, A. F.; Chu, S. N. G.; Wilson, R. G.; Zavada, J. M.; Polyakov, A. Y.; Osinsky, A. V.; Norris, P. E.; Chow, P. P.; Wowchack, A. M.; Hove, J. M. V.; Park, Y. D. *J. Vac. Sci. Technol., A* **2002**, *20* (3), 721–724. (c) Coey, J. M. D.; Devlin, E.; Gambino, R. J. *J. Appl. Phys.* **1982**, *53*, 7810–7812.

(17) Zając, M.; Gosk, J.; Grzanka, E.; Stelmakh, S.; Palczewska, M.; Wysmołek, A.; Korona, K.; Kamińska, M.; Twardowski, A. *J. Alloys Compd.* **2008**, *456*, 324–338.

(18) (a) Akinaga, H.; Nemeth, S.; DeBoeck, J.; Nistor, L.; Bender, H.; Borghs, G.; Ofuchi, H.; Oshima, M. *Appl. Phys. Lett.* **2000**, *77* (26), 4377–4379. (b) Theodoropoulou, N.; Hebard, A. F.; Overberg, M. E.; Abernathy, C. R.; Pearton, S. J.; Chu, S. N. G.; Wilson, R. G. *Appl. Phys. Lett.* **2001**, *78* (22), 3475–3477.

(19) Alves, E.; Liu, C.; Waerenborgh, J. C.; da Silva, M. F.; Soares, J. C. *Nucl. Instrum. Methods Phys. Res., Sect. B* **2001**, *175*−*177*, 241–245.

(20) Jiraskova, Y.; Havlicek, S.; Schneeweiss, O.; Periña, V.; Blawert, C. *J. Magn. Magn. Mater.* **2001**, *234*, 477–488.

(21) Gajbhiye, N. S.; Bhattacharyya, S.; Shivaprasad, S. M. *Mater. Res. Bull.* **2008**, *43*, 272–283.

(22) (a) Rodriguez-Carvajal, J. *Physica B* **1993**, *192*, 55–69. (b) Rodriguez-Carvajal, J. *FULLPROF*, version 4.0; Institut Laue-Langevin: Grenoble, France, 2007.

(23) Brand, R. A. *Mössbauer spectra analysis program*, Win Normos Version 3.00; supplied by Wissel: Germany May 2009.

(24) (a) Hohenberg, P.; Kohn, W. *Phys. Rev.* **1964**, *136*, B864–B871. (b) Kohn, W.; Sham, L. J. *Phys. Rev.* **1965**, *140*, A1138. (c) Singh, D. *Plane Waves Pseudopotentials and the LAPW Method*; Kluwer Academic Publishers: London, 1994. (d) Martin, R. M. *Electronic Structure, Basic Theory and Practical Methods*; Cambridge University Press: NewYork, 2004.

(25) Blaha, P.; Schwarz, K.; Luitz, J.; Madsen, G. K. H.; Kvasnicka, D. *WIEN2K*; Technical University of Vienna: Vienna, Austria, 2001.

(26) Perdew, J. P.; Burke, S.; Ernserhof, M. *Phys. Rev. Lett.* **1996**, *77*, 3865–3868.

JP106221W